

Joseph C. McGinley
Neil Roach
John P. Gaughan
Scott H. Kozin

Forearm interosseous membrane imaging and anatomy

Received: 2 February 2004
Revised: 1 April 2004
Accepted: 2 April 2004
Published online: 25 August 2004
© ISS 2004

J. C. McGinley
School of Medicine,
Temple University,
Philadelphia, Pennsylvania, USA

N. Roach
Department of Radiology,
Hospital of the University of Pennsylvania,
Philadelphia, Pennsylvania, USA

J. P. Gaughan
Department of Biostatistics,
Temple University,
Philadelphia, Pennsylvania, USA

S. H. Kozin (✉)
Pediatric Hand & Upper Extremity Surgery,
Shriners Hospitals for Children,
3551 N Broad Street, Philadelphia,
PA 19140, USA
e-mail: skozin@shrinenet.org
Tel.: +1-215-4304034
Fax: +1-215-4304079

S. H. Kozin
Department of Orthopaedic Surgery,
Temple University,
Philadelphia, Pennsylvania, USA

Abstract *Objective:* To determine the regional thickness variation of the interosseous membrane (IOM) along the forearm and validate magnetic resonance imaging of the IOM with laser micrometry. *Design and patients:* Axial thickness measurements of 12 cadaver forearms were obtained using magnetic resonance imaging (MRI) at radial, central, and ulnar locations. The specimens were dissected, and IOM thickness measured using a laser micrometer. MRI and laser measurements of the main and oblique IOM bundles were compared. An axial thickness profile was plotted versus forearm length, and radial, central, and ulnar positions were compared. *Results:* The main bundle thickness was 2.18 ± 0.20 mm using laser micrometry, which was not significantly different from MRI measurements (1.86 ± 0.25 mm, $p=0.11$, power = 0.84). The dorsal oblique bundle thickness was not significantly different between measurement methods (2.93 ± 0.77 mm and 3.30 ± 1.64 mm using laser micrometry and MRI respectively,

$p=0.75$, power = 0.04). Both methods demonstrated a progressive increase in thickness proximally within the forearm. MRI measurements demonstrated a significantly greater thickness increase in the radial location compared to the central location (slope = 2.26 and 1.05, $r^2=0.31$ and 0.12 respectively, $p<0.05$). The ulnar slope was not significantly different from zero ($r^2=0.02$, $p>0.05$). *Conclusion:* Our findings describe the varying IOM anatomy using MRI, and determined the location of the clinically important IOM fiber bundles. This study confirms the accuracy of MR imaging of the IOM by comparison with a laser micrometer, and demonstrates the thickness variation along the forearm. This information may be used to identify changes in IOM anatomy with both acute IOM injury and chronic fiber attenuation.

Keywords Magnetic resonance · Anatomy · Radius · Ulna · Soft tissues · Ligaments

Introduction

The interosseous membrane (IOM) is a dynamic and complex fibrous structure within the forearm. The IOM maintains longitudinal forearm stability, transmits forces from the radius to the ulna and is the origin of several muscle groups [1, 2]. The IOM is composed of three anterior components and two posterior components [3].

The disruption of IOM function following forearm trauma varies based on the location and chronicity of the injury.

Each anatomic section of the IOM maintains a different component of forearm stability. Following radial head resection, the anterior central bundle was responsible for 71% of the longitudinal stiffness of the IOM [4]. The posterior oblique bundle contributes to the stability of the proximal radio-ulnar joint, while the distal horizontal

fibers maintain distal radio-ulnar joint stability [3]. Nakamura et al. [5] described the geometric variation of the distal fibers, suggesting a dynamic function during forearm rotation.

The strength and mechanics of each anatomic location of the IOM depends on the fiber bundle geometry and orientation. Several authors have previously described the IOM anatomy using varying imaging techniques [5, 6, 7, 8, 9, 10]. The purpose of this study was: (1) to validate the accuracy of MR imaging of the IOM when compared to measurements obtained using a laser micrometer, (2) describe the anatomy of the central and oblique fiber bundles, and (3) compare the membrane thickness distribution along the length of the forearm at radial, central and ulnar locations.

Materials and methods

MRI protocol

Twelve fresh-frozen cadaver upper extremities (60–86 years, mean 73 years), precut at the mid-humerus level, were thawed in a warm isotonic saline solution. Each upper extremity was braced in elbow extension and forearm supination for imaging studies on a 1.5 Tesla MR scanner (GE Medical Systems, Milwaukee, WI, USA). Axial FSE images were obtained utilizing a torso coil with a repetition time (TR) of 3550 ms, an echo time (TE) of 89 ms, a field of view (FOV) of 12×12 cm with a 256×256 matrix. The slice thickness was 5 mm with a 2-mm skip. Thirty-five images were obtained for each specimen and reviewed on an AGFA IMPAX workstation (Gevaert, Mortsel, Belgium). The length of the radius was measured on a coronal scout image using an electronic caliper. The position of each axial image measurement was expressed as a percentage distance from the radial styloid process to the radial

head. The axial images closer than the midpoint of the radius (closer to the radial styloid) are less than 0.5. The axial images distal to the midpoint of the radius (closer to the radial head) are greater than 0.5. Each slice was reviewed and the thickness of the IOM was measured at the radial, central and ulnar locations (Fig. 1). The thickness of each section was grouped by location and plotted against the position along the radius. The central fiber bundle of the IOM was determined by locating the largest thickness measurements with a distal oblique direction from the radius to the ulna (Fig. 1). Similarly, the dorsal oblique bundle was determined by locating the largest thickness measurements with a proximal oblique direction from the radius to the ulna (Fig. 1).

Laser measurements

The humerus and hand were removed from each upper extremity. The forearms were dissected removing all soft tissue down to the radius, ulna and IOM. The IOM was viewed under a dissecting microscope at a magnification of 40X and any additional soft tissue was removed. The length of the radius was measured using a digital caliper, and thickness measurements were made along the length of the radius. The specimens were clamped in a supinated position and a SK-031 laser system connected to a RD controller (Keyence Corp, Saddlebrook, NJ, USA) was positioned on both sides on the IOM (Fig. 2). The thickness measurement range of the laser system was set at an upper limit of five millimeters with a resolution of one micron and a spot diameter of thirty microns. The system linearity was $\pm 0.1\%$ of full scale with a sampling time of 512 μs (technical specification for SK-031 CCD laser displacement sensor; Keyence Corp). Axial IOM thickness measurements were obtained at 3.2-mm intervals at radial, central and ulnar locations along the entire length of the radius. The distance between measurements was limited by the laser-attachment slot spacing. The thickness of the IOM was grouped by location and plotted against the position along the radius. The main and dorsal oblique bundles were identified for each specimen.

Fig. 1 A The IOM is composed of several anatomic locations. Distally the membrane is very thin without discrete fiber bundles. At the mid-forearm level, there are several accessory fiber bundles demonstrating distinct orientation from the radius to their ulnar insertion. Just proximal to the mid-forearm is the location of the main fiber bundle. On the dorsal aspect of the proximal forearm the oblique bundle has its origin on the ulna and inserts distally on the radius. The *dashed line* indicates the level of the axial image in **B**. **B** Thickness measurements were obtained using laser and MRI at three locations: ulnar, central, and radial. This image demonstrates the various measurement locations at the mid-forearm level

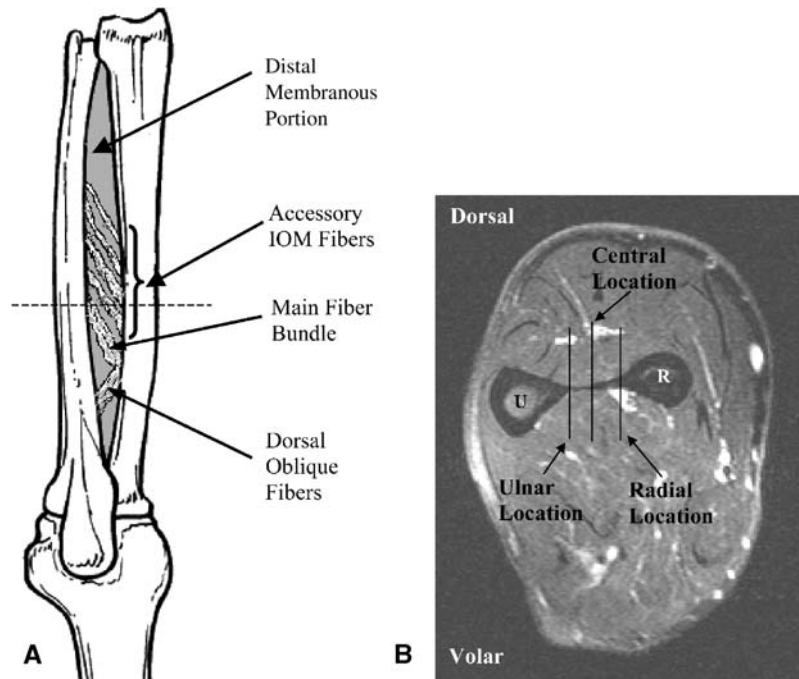
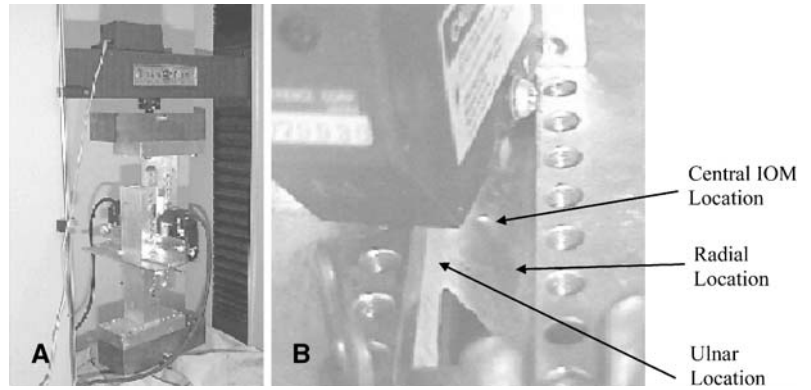


Fig. 2 **A** Laser system setup. The laser was positioned perpendicular to the interosseous membrane and advanced in 3.2 mm increments using the slots in the apparatus. **B** IOM measurements were obtained at ulnar, central, and radial locations. The *white area* in the central location illustrates the laser-beam measurement location



Statistical methods

Measurement methods were compared using a generalized linear model followed by pair-wise comparisons of means using the Bonferroni adjustment to maintain an experiment-wise error of 0.05. Least-squares linear regression was used to evaluate the relationship between normalized distance and thickness. Slopes were compared using 95% confidence intervals.

Results

Table 1 summarizes the results of the average axial-thickness measurements of the main and oblique fiber bundles using MRI and laser methods. Fig. 3 illustrates the normal cross-sectional IOM anatomy and thickness variability at several points along the length of the radius. Fig. 4 demonstrates the location and anatomy of the oblique fiber bundle in the sagittal section. The main bundle thickness was 2.18 ± 0.20 mm (avg. \pm SD) using laser micrometry ($n=9$) and was not significantly different from MRI measurements (1.86 ± 0.25 mm, $n=10$, $p=0.1054$, power = 0.84). The dorsal oblique bundle thickness was found to equal 2.93 ± 0.77 mm using laser micrometry ($n=57$) and 3.30 ± 1.64 mm using MRI ($n=4$). There was no significant difference between measurement methods ($p=0.75$, power = 0.04).

Thickness values versus location along the radius were plotted at radial, central and ulnar locations using MRI and laser methods. The slope of each graph was determined as the change in thickness measurement divided by the change in location along the radius (Figs. 5 & 6). Both methods demonstrated an increased thickness proximally within the forearm at radial and central locations (positive slope). Using MRI, the slope of the thickness-position

relationship was 2.26, 1.05 and 0.50 at radial, central and ulnar locations respectively ($r^2=0.31$, 0.12 and 0.02 respectively). The radial slope was significantly larger than the central slope. The slope of the ulnar location was not significantly different from zero ($r^2=0.02$). Laser micrometry demonstrated no significant difference between the radial, central and ulnar thickness slopes (2.81, 2.60 and 1.86 respectively, $r^2=0.40$, 0.40 and 0.17 respectively).

Discussion

The complex anatomy of the IOM results in a structure capable of numerous physiologic functions. Disruption of the fiber bundles of the IOM may result in longitudinal forearm instability, a decreased range of rotational motion, a reduction in grip strength, or chronic pain and disability based upon the location of the injury. Several authors have described the gross anatomic arrangement of the IOM. The IOM is composed of a distal membranous portion, several accessory bundles, a larger main fiber bundle, and a proximal dorsal oblique bundle. The number of accessory bundles varies from one to five, and the dorsal oblique bundle occurs in approximately 85% of the specimens [11]. The IOM bundles originate from the radius 7.3–16.2 cm distal to the radial head and insert onto the ulna 6.4–13.7 cm distal to the olecranon [12]. The fibers traverse the interosseous space at an average angle of twenty degrees [12]. The IOM has been shown to be most taut in a neutral rotational position, demonstrating the dynamic variability within the membrane [13].

Table 1 IOM thickness comparison data

Bundle	Method	Measurements	Location (percent distance)	Thickness (mm)
Main	MRI	9	0.57 ± 0.07	1.86 ± 0.25
Main	Laser	9	0.62 ± 0.03	2.18 ± 0.20
Oblique	MRI	4	0.64 ± 0.03	3.30 ± 1.64
Oblique	Laser	57	0.67 ± 0.06	2.93 ± 0.77

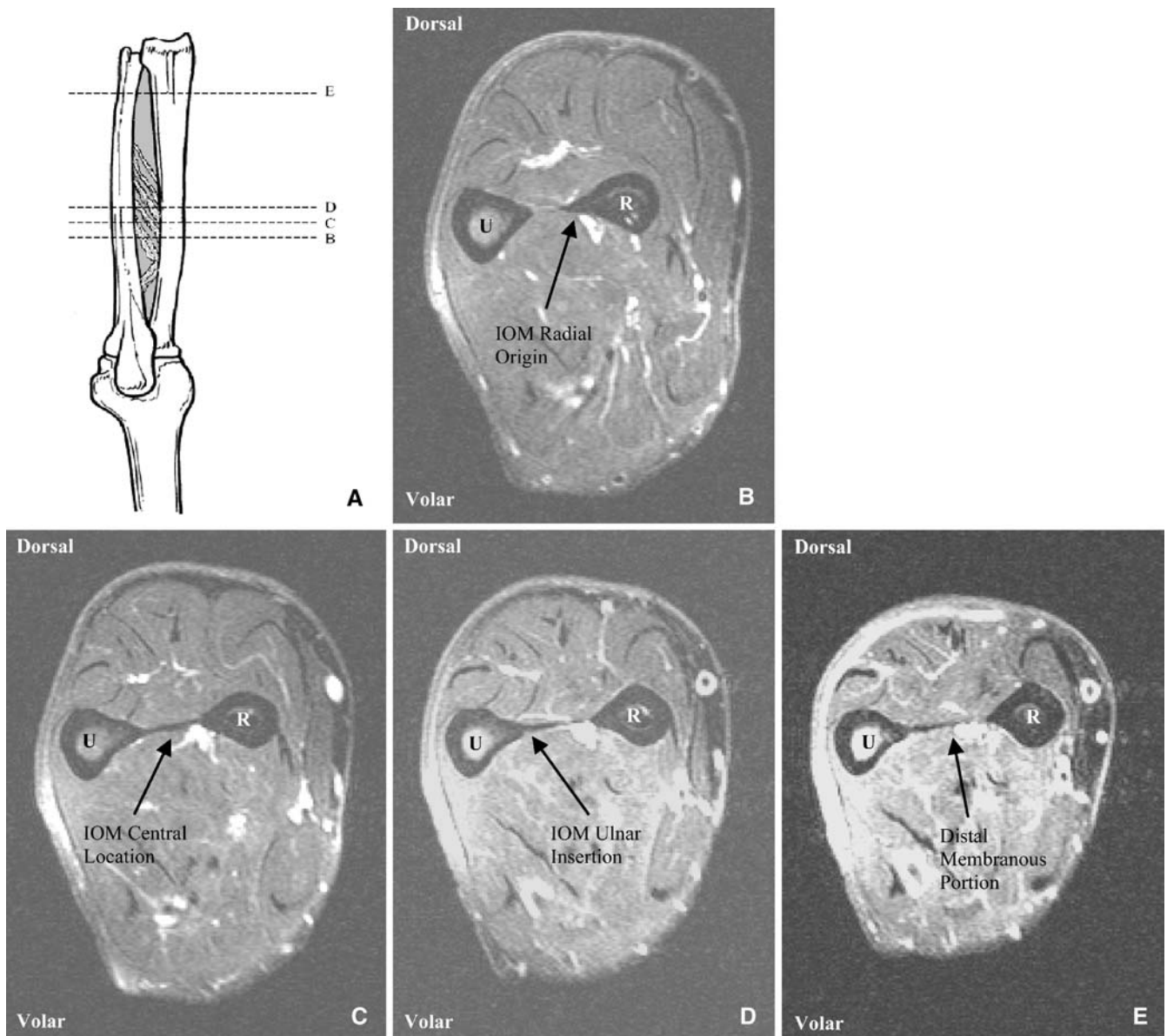


Fig. 3A–E Axial FSE image of the intact forearm specimen obtained utilizing a torso coil with TR of 3550 ms, TE of 89 ms, and FOV of 12×12 cm with a 256×256 matrix. The slice thickness was 5 mm with a 2-mm skip. **A** This illustration demonstrates the location along the radius of the following axial MRI images of the IOM. **B** The main fiber bundle originates from the proximal radius.

C The central location of the main fiber bundle is demonstrated in this image, just distal to its origin. **D** The main fiber bundle inserts onto the ulna just proximal to the mid-forearm level. **E** The distal membranous portion is a thin fibrous structure without any distinct bundles

Recent studies have investigated the use of ultrasound and magnetic resonance imaging to describe the anatomy of the IOM and diagnose traumatic injury. Ultrasound analysis of tibiofibular IOM injury in 90 ankle fractures demonstrated a sensitivity of 89%, a specificity of 95% and a diagnostic value of 92% compared to intraoperative diagnosis [14]. Failla et al. [6] demonstrated that ultrasound could accurately diagnose and identify lesions to the antebrachial IOM in several cadavers and patients.

The IOM was very hyperechoic, and disruption was easily identifiable on ultrasound [6].

Several papers by Nakamura et al. have investigated the use of MRI in identifying the static and dynamic variability of the IOM [5, 7, 8]. Three-dimensional imaging of the IOM demonstrated wavy deformities in pronation and dorsiflexion of the IOM in supination, occurring primarily in the distal membranous location [7]. The IOM maintained a flat orientation in neutral rotation

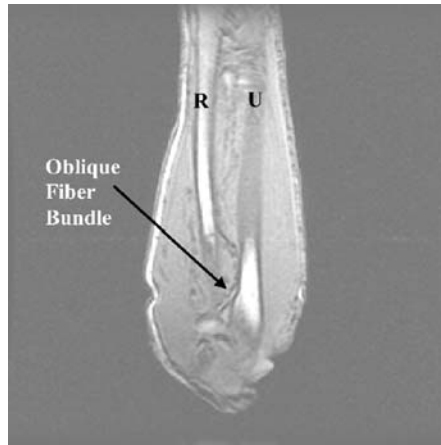


Fig. 4 Sagittal images of the forearm demonstrated the extent and structure of the dorsal oblique fiber bundle of the IOM. The oblique bundle originates from the proximal ulna, and inserts distally onto the radius

[7]. The interosseous distance and IOM length were found to be maximal from a neutral to slightly-supinated position [8]. IOM anatomy and injury can most accurately be visualized using axial T2-weighted fast spin-echo images with fat suppression [9].

The purpose of our study was to confirm the accuracy of MR imaging of the IOM and describe the varying anatomic thickness distribution of the membrane. MRI provides a non-invasive and safe diagnostic tool for evaluation the IOM. However, the resolution and precision of these images has not been thoroughly evaluated. The results of this study demonstrated that magnetic resonance could accurately depict small differences in thickness within the IOM. There was no significant difference between the thickness values obtained using MRI or laser micrometry.

The unique anatomic variability of the IOM results in a complex mechanical structure. The relative thickness of the membrane throughout the forearm contributes to force distribution and longitudinal forearm stability. We have shown that the IOM thickness pattern varies greatly throughout the forearm using MRI and laser micrometry. The thickness pattern also varied based on membrane location (radial origin, central mid-substance, ulnar insertion). Previous studies have measured discrete locations of membrane thickness using mechanical calipers demonstrating a maximal thickness of 0.94 ± 0.2 mm located just proximal to the midpoint of the radius [4]. Our results suggest the reported data under-represent actual thickness values, and the difference may be due to compression artifact with the use of mechanical calipers. The dorsal oblique band was found to be the largest fiber bundle within the IOM. The increased size of this bundle and its location suggests that it withstands large loads and

may play a role in the maintenance of proximal forearm stability.

When comparing the location and thickness patterns of the IOM, measurements were obtained using 5 mm increments with a 2 mm skip on MRI, while laser measurements were obtained at 3.2 mm intervals. The differences in measurement locations occurred due to limitations in the experimental setup. The laser system was only capable of measurements at 3.2 mm intervals. All MRI scans were performed prior to laser measurements, using a standard imaging protocol. The differences in measurement location do not affect the comparison of the data, based on the quantity of points obtained and the focus on measurements of specific fiber bundles. The effects of volume averaging on IOM thickness measurements were evaluated by initially using 3 mm slices. At this slice thickness, the scanning time was excessive. The slice thickness was changed to 5 mm without any measurable difference in data values. Chemical-shift artifact was initially observed when using volume gradient echo imaging. To reduce this artifact, our protocol was changed to FSE T2-weighted sequences, thereby decreasing chemical-shift artifact. An extremity coil was initially used in our study. The extremity coil provides increased spatial resolution compared to the torso coil. However, the extremity coil was limited due to signal drop-off at the proximal and distal aspects of the forearm. We compared proton density with T2-weighted images and found in cadavers, T2-weighted images demonstrated increased anatomic detail of the IOM.

Surgical reconstruction of the interosseous membrane has been done. In cadavers, a flexor carpi radialis graft was used to reconstruct the central band of the interosseous membrane and this reduced radial migration [15]. Another surgeon has performed a repair of the interosseous. Favorable results were reported at short-term follow-up [6].

In summary, we have shown IOM thickness values obtained using MRI did not significantly differ from values obtained using laser micrometry. We demonstrated the variability of the IOM along the length of the forearm at radial, central and ulnar locations and found the proximal membrane to be thicker than the distal membrane. This information provides important anatomic descriptions which may be useful in analyzing IOM function and injury. In cases of acute forearm trauma, assessment of IOM integrity may be performed by visualizing the oblique bundle, the main bundle, and the continuity of the distal membranous fibers. By knowing the relative location, size and anatomy of each of these structures, a thorough analysis of the IOM can be performed. The thickness distribution is relevant in evaluating the IOM in cases of chronic failure following radial-head resection or replacement. Without the radial head as the primary longitudinal forearm stabilizer, the fibers of the IOM become attenuated over time, resulting in the proximal

Fig. 5 Laser micrometer thickness measurements plotted against percentage distance along the radius and central, ulnar, and radial positions. There was a progressive increase in membrane thickness proximally along the radius, as demonstrated by the positive slope at all three locations. (A central, B ulnar, C radial)

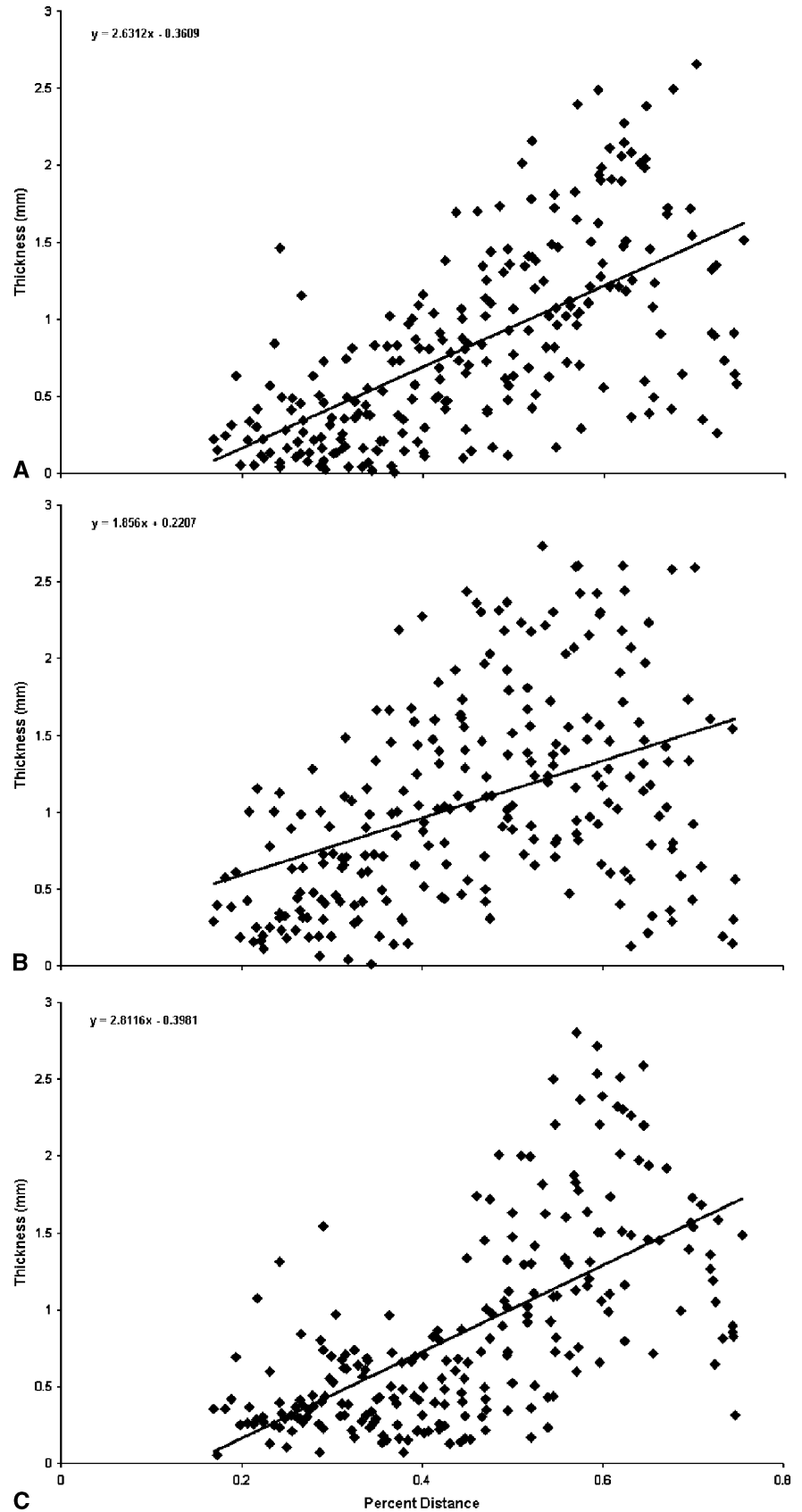
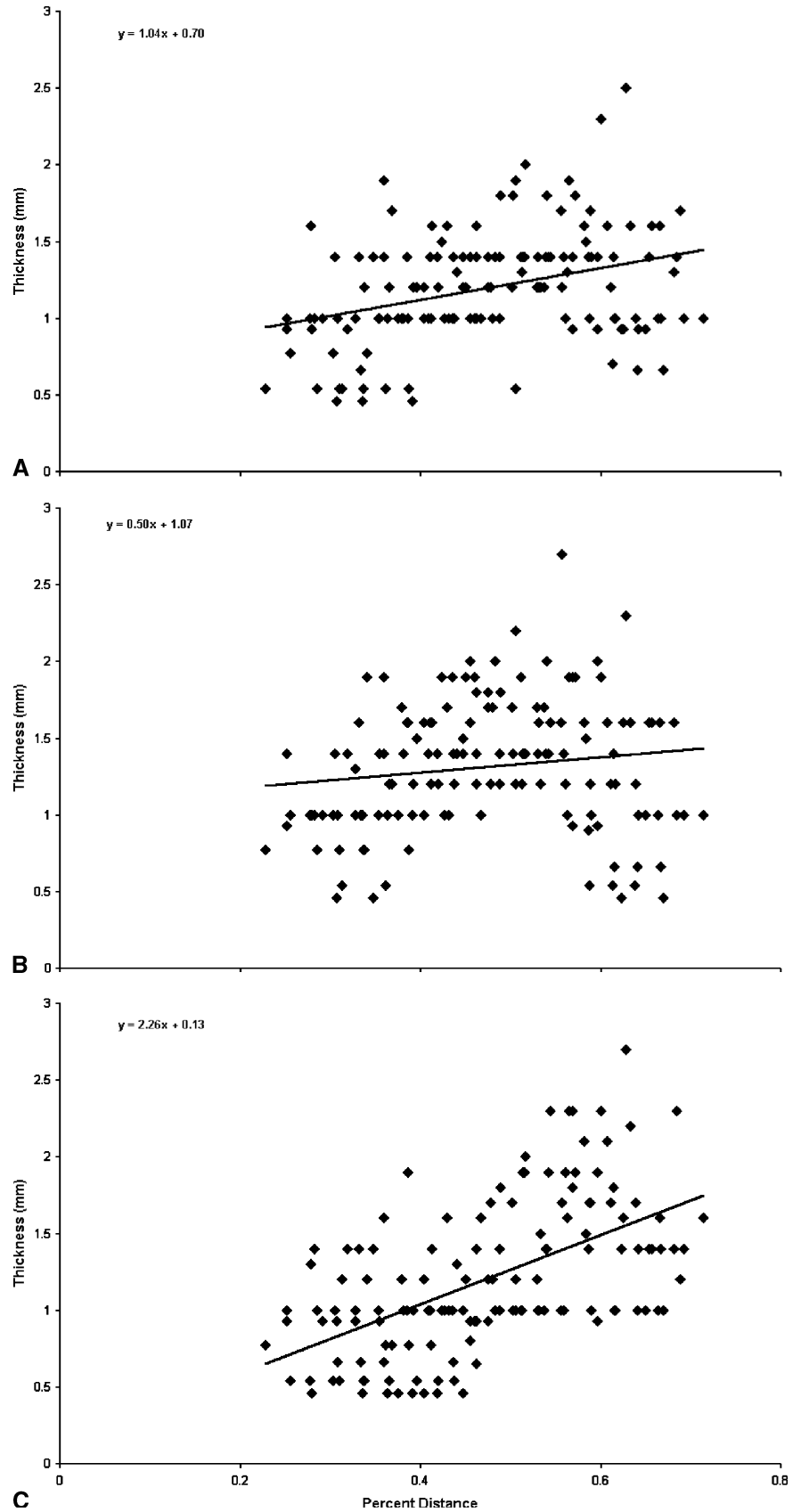


Fig. 6 MRI thickness measurements plotted against percent distance along the radius and central, ulnar, and radial positions. IOM thickness was found to be greater proximally along the radius as indicated by the positive linear relation (slope). (A central, B ulnar, C radial)



migration of the radius and positive ulnar variance. By determining the thickness of the membrane along its length, an assessment of chronic failure can be performed. The IOM represents a complex anatomic structure with several physiologic functions. Acute and chronic membrane failure can be assessed by evaluating important anatomic landmarks and by determining the fiber thickness distribution.

References

- Hollister AM, Gellman H, Waters RL. The relationship of the interosseous membrane to the axis of rotation of the forearm. *Clin Orthop* 1994; 298:272–276.
- Werner JA, Koebke J. The function of the antebrachial interosseous membrane. *Anat Embryol* 1987; 176:127–131.
- Poitevin LA. Anatomy and biomechanics of the interosseous membrane: its importance in the longitudinal stability of the forearm. *Hand Clin* 2001; 17:97–110.
- Hotchkiss RN, An KN, Sowa DT, Basta S, Weiland AJ. An anatomic and mechanical study of the interosseous membrane of the forearm: pathomechanics of proximal migration of the radius. *J Hand Surg [Am]* 1989; 14:256–261.
- Nakamura T, Yabe Y, Horiuchi Y. Functional anatomy of the interosseous membrane of the forearm - dynamic changes during rotation. *Hand Surg* 1999; 4:67–73.
- Failla JM, Jacobson J, van Holsbeeck M. Ultrasound diagnosis and surgical pathology of the torn interosseous membrane in forearm fractures/dislocations. *J Hand Surg [Am]* 1999; 24:257–266.
- Nakamura T, Yabe Y, Horiuchi Y, Yamazaki N. Three-dimensional magnetic resonance imaging of the interosseous membrane of forearm: a new method using fuzzy reasoning. *Magn Reson Imaging* 1999; 17:463–470.
- Nakamura T, Yabe Y, Horiuchi Y. In vivo MR studies of dynamic changes in the interosseous membrane of the forearm during rotation. *J Hand Surg [Br]* 1999; 24:245–248.
- Starch DW, Dabezies EJ. Magnetic resonance imaging of the interosseous membrane of the forearm. *J Bone Joint Surg Am* 2001; 83:235–238.
- Jaakkola JI, Riggans DH, Lourie GM, Lang CJ, Hassem BE, Rosenthal SJ. Ultrasonography for the evaluation of forearm interosseous membrane disruption in a cadaver model. *J Hand Surg [Am]* 2001; 26:1053–1057.
- Skahen JR 3rd, Palmer AK, Werner FW, Fortino MD. The interosseous membrane of the forearm: anatomy and function. *J Hand Surg [Am]* 1997; 22:981–985.
- Schneiderman G, Meldrum RD, Bloebaum RD, Tarr R, Sarmiento A. The interosseous membrane of the forearm: structure and its role in Galeazzi fractures. *J Trauma* 1993; 35:879–885.
- Christensen JB, Adams JP, Cho KO, Miller L. A study of the interosseous distance between the radius and ulna during rotation of the forearm. *Anat Rec* 1968; 160:261–271.
- Christodoulou G, Korovessis P, Giarmenitis S, Dimopoulos P, Sdougos G. The use of sonography for evaluation of the integrity and healing process of the tibiofibular interosseous membrane in ankle fractures. *J Orthop Trauma* 1995; 9:98–106.
- Skahen JR III, Palmer AK, Werner FW, Fortino MD. Reconstruction of the interosseous membrane of the forearm in cadavers. *J Hand Surg [Am]* 1997; 22:986–994.